Simulation of Channel Flows Using Thermal Lattice Boltzmann Method

S. Gokaltun [a]

[a] *Florida International University, Applied Research Center, EC 2100, 10555 W Flagler St, Miami, FL 33174, USA*

G.S. Dulikravich [b,*]

[b] *Florida International University, Department of Mechanical and Materials Engineering, Multidisciplinary Analysis, Inverse Design, Robust Optimization and Control (MAIDROC) Lab., EC 3474, 10555 W Flagler St, Miami, FL 33174, USA*

Abstract

A thermal lattice Boltzmann method (TLBM) is used for analysis of flow and heat transfer in two-dimensional channels. Simulation results are presented for thermal Couette and thermal Poiseuille channel flows. Analytical solution for temperature field in hydraulically and thermally developed flows are used to verify the current TLBM results. The method is further applied to study the forced convection in a channel flow with a square blockage acting as the cooling source. The effects of the size and temperature of the square block is investigated. We conclude that the LBM method can be used as an alternative numerical model to study channel flows with heat transfer.

Key words: lattice Boltzmann method, heat transfer, channel flow

Preprint submitted to Computers & Mathematics with Applications24 September 2008

1 Introduction

Lattice Boltzmann method has been introduced to the scientific community as a new alternative numerical method that can solve for flows with complex physics [1] however there are still areas that need to be studied in order to obtain a well established LBM. One aspect of this improvement is the solution of flows with heat transfer [2, 3]. In an effort to obtain a thermal lattice Boltzmann method (TLBM), a variety of techniques were proposed in the literature, namely the multi-speed approach, the passive-scalar approach and the double populations approach. The model developed by He *et al.* [4] has gained the most popularity because it was more stable and it had the capability to solve for viscous dissipation and compression work. In this model, the thermal lattice Boltzmann equation was derived by discretizing the Boltzmann equation for the internal energy distribution. As a result, thermal energy and heat flux were able to be obtained by taking the kinetic moments of the thermal energy distribution function. The method proposed by He *et al.* [4] was accepted by many researchers and it was successfully applied to solve for various kinds of fluid flow problems with heat transfer. Dixit and Babu [5] used this model to simulate natural convection of a Boussinesq fluid in a square cavity. It was demonstrated that for high Rayleigh numbers the TLBM results agreed well with other benchmark numerical simulations. Tang et al. [6] proposed boundary conditions to improve the same model in order to solve for two-dimensional Poiseuille and Couette flow and verified the TLBM results with Finite Volume Method and analytical solutions at various wall boundary conditions. D'Orazio

* Corresponding author.
Email addresses: gokaltun@fiu.edu (S. Gokaltun), dulikrav@fiu.edu (G.S. Dulikravich).

and Succi [7] introduced a counter-slip internal energy boundary condition for the TLBM model and obtained satisfactory results for hydrodynamically and thermally developed channel flows heated at the inlet. In their simulations the TLBM was able to capture the effect of viscous dissipation which was tested for thermal Couette flow at various Brinkmann numbers. There have been a couple of studies that aimed to implement the TLBM in fluid flow and heat transfer in complex geometries. Huang *et al.* [8] solved the natural convection in a concentric annulus involving circular solid boundaries. The curved non-slip wall boundary treatment for isothermal LBM [9] was extended to treat the thermal curved solid boundary in the two-population TLBM computations. Chen et al. [10] applied the same boundary condition for two-dimensional solutions of backward-facing step flows with inclined plates positioned along the flow field at various angles. Gokaltun and Dulikravich [11] verified the TLBM solutions for a constricted channel flow against against FEM solutions for velocity and thermal fields. The purpose of this study is to present the capability of TLBM in simulation of incompressible fluid flow and heat transfer in channels with various flow conditions. First the governing equations and the numerical solution algorithm are presented. Next the velocity and temperature boundary conditions used for open and solid boundaries are introduced. The results are then presented and discussed in Section 3. The present TLBM method is first validated for two-dimensional straight channels where the results are compared with analytical solutions. Then the method is applied to solve for forced convection in a channel with a square blockage. Interactions of the blockage size and the blockage temperature on the flow characteristics are also studied. Finally, some conclusions are drawn in Section 4.

2 Numerical Method

In this paper, He's thermal lattice Boltzmann model [4] is adopted to solve for the heat transfer in channel flows. The TLBM solves the following discrete evolution equations:

$$\tilde{f}_a(\mathbf{x}+\mathbf{e_a}\Delta t, t+\Delta t) = \tilde{f}_a(\mathbf{x},t) - \frac{\Delta t}{\tau_p + 0.5\Delta t}\left(\tilde{f}_a(\mathbf{x},t) - f_a^{eq}(\mathbf{x},t)\right), \tag{1}$$

$$\begin{aligned}\tilde{g}_a(\mathbf{x}+\mathbf{e_a}\Delta t, t+\Delta t) = \tilde{g}_a(\mathbf{x},t) &- \frac{\Delta t}{\tau_g + 0.5\Delta t}\left(\tilde{g}_a(\mathbf{x},t) - g_a^{eq}(\mathbf{x},t)\right) \\ &- \frac{\tau_g \Delta t}{\tau_g + 0.5\Delta t} f_a(\mathbf{x},t) h_a(\mathbf{x},t).\end{aligned} \tag{2}$$

where

$$\tilde{f}_a(\mathbf{x},t) = f_a(\mathbf{x},t) - \frac{\Delta t}{2\tau_p}\left(f_a^{eq}(\mathbf{x},t) - f_a(\mathbf{x},t)\right), \tag{3}$$

$$\tilde{g}_a(\mathbf{x},t) = g_a(\mathbf{x},t) - \frac{\Delta t}{2\tau_g}\left(g_a^{eq}(\mathbf{x},t) - g_a(\mathbf{x},t)\right) + \frac{\Delta t}{2} f_a(\mathbf{x},t) h_a(\mathbf{x},t). \tag{4}$$

In Eq. (4), the term h_a represents the effect of viscous heating and can be expressed as

$$h_a(\mathbf{x},t) = (\mathbf{e_a} - \mathbf{u}) \cdot [-\nabla(\frac{P}{\rho}) + \frac{1}{\rho}\nabla \cdot \Pi + (\mathbf{e_a} - \mathbf{u}) \cdot \nabla \mathbf{u}], \tag{5}$$

which can be reduced to [6]

$$h_a(\mathbf{x},t) = (\mathbf{e_a} - \mathbf{u}) \cdot [\partial_t \mathbf{u} + (\mathbf{e} \cdot \nabla)\mathbf{u}]. \tag{6}$$

In D'Orazio et al. [3], Eq. (6) is given as:

$$h_a(\mathbf{x},t) = (\mathbf{e_a} - \mathbf{u}(\mathbf{x},t)) \cdot \left[\mathbf{u}(\mathbf{x}+\mathbf{e_a}\Delta t, t+\Delta t) - \mathbf{u}(\mathbf{x},t)\right]/\Delta t, \tag{7}$$

which is used in this work to calculate h_a. The new distribution variables $\tilde{f}$ and $\tilde{g}$ are related to old variables f and g as given below:

$$\tilde{f}_a = f_a + \frac{0.5\Delta t}{\tau_p}(f_a - f_a^{eq}), \tag{8}$$

$$\tilde{g}_a = g_a + \frac{0.5\Delta t}{\tau_g}(g_a - g_a^{eq}) + \frac{\Delta t}{2} f_a h_a. \tag{9}$$

The equilibrium density distribution functions for f and g are given as follows:

$$f_a^{eq} = w_a \rho \left[1 + 3\frac{\mathbf{e}_a \cdot \mathbf{u}}{c^2} + \frac{9}{2}\frac{(\mathbf{e}_a \cdot \mathbf{u})^2}{c^4} - \frac{3}{2}\frac{\mathbf{u^2}}{c^2}\right], \tag{10}$$

$$g_{1-4}^{eq} = w_{1-4} \rho e(\mathbf{x}) \left[\frac{3}{2} + \frac{3}{2}\frac{\mathbf{e}_a \cdot \mathbf{u}}{c^2} + \frac{9}{2}\frac{(\mathbf{e}_a \cdot \mathbf{u})^2}{c^4} - \frac{3}{2}\frac{\mathbf{u^2}}{c^2}\right], \tag{11}$$

$$g_{5-8}^{eq} = w_{5-8} \rho e(\mathbf{x}) \left[3 + 6\frac{\mathbf{e}_a \cdot \mathbf{u}}{c^2} + \frac{9}{2}\frac{(\mathbf{e}_a \cdot \mathbf{u})^2}{c^4} - \frac{3}{2}\frac{\mathbf{u^2}}{c^2}\right], \tag{12}$$

$$g_9^{eq} = w_9 \rho e(\mathbf{x}) \left[-\frac{3}{2}\frac{\mathbf{u^2}}{c^2}\right]. \tag{13}$$

The weighting coefficients in Eq. (10-13) are selected as $w_{1-4} = 1/9$, $w_{5-8} = 1/36$ and $w_9 = 4/9$. The D2Q9 lattice structure used in this study is shown in Fig. 1, where particles move along 9 specific directions with speed

$$\mathbf{e_a} = \begin{cases} (\cos[(a-1)\frac{\pi}{2}], \sin[(a-1)\frac{\pi}{2}])c, & a = 1-4 \\ (\cos[(a-5)\frac{\pi}{2} + \frac{\pi}{4}], \sin[(a-5)\frac{\pi}{2} + \frac{\pi}{4}])c, & a = 5-8 \\ (0,0), & a = 9 \end{cases} \tag{14}$$

The ninth velocity is zero which stands for the particles at rest. The length scale ($1\ lu$) is fixed by the distance between nodes. The macroscopic density ρ, velocity $\mathbf{u}$, internal energy per unit mass e, heat flux $\mathbf{q}$, are obtained by the following relations:

$$\rho = \sum_a \tilde{f}_a, \tag{15}$$

$$\rho \mathbf{u} = \sum_a \mathbf{e}_a \tilde{f}_a, \tag{16}$$

$$\rho e = \sum_a \tilde{g}_a - \frac{\Delta t}{2}\sum_a f_a h_a, \tag{17}$$

$$\mathbf{q} = \left(\sum_a \mathbf{e}_a \tilde{g}_a - \rho e \mathbf{u} - \frac{\Delta t}{2} \sum_a \mathbf{e}_a f_a h_a \right). \tag{18}$$

Kinematic viscosity is given by $\nu = \tau_p R T_0$, and thermal diffusivity is given by $\chi = 2\tau_g R T_0$ and internal energy is related to temperature by $\rho e = \rho R T$ in 2D.

2.0.1 Thermal LBM Procedure

The solution of the TLB equations given by Eq. (2) and Eq. (3) is carried in two steps: (a) collision and (b) streaming. The collision step calculates the right hand side of Eq. (2) and Eq. (3) and assigns the value to buffer parameters, $\tilde{f}_a^*$ and $\tilde{g}_a^*$ by

$$\tilde{f}_a^*(\mathbf{x}, t) = (1 - \omega_f)\tilde{f}_a(\mathbf{x}, t) + \omega_f f_a^{eq}(\mathbf{x}, t), \tag{19}$$
$$\tilde{g}_a^*(\mathbf{x}, t) = (1 - \omega_g)\tilde{g}_a(\mathbf{x}, t) + \omega_g g_a^{eq}(\mathbf{x}, t) - \omega_g \tau_g f_a h_a, \tag{20}$$

where $\omega_f = \Delta t/(\tau_f + 0.5\Delta t)$ and $\omega_g = \Delta t/(\tau_g + 0.5\Delta t)$. The distribution functions at the new time level are then streamed to the neighboring nodes in the streaming step by

$$\tilde{f}_a(\mathbf{x} + \mathbf{e}_a \Delta t, t + \Delta t) = \tilde{f}_a^*(\mathbf{x}, t), \tag{21}$$
$$\tilde{g}_a(\mathbf{x} + \mathbf{e}_a \Delta t, t + \Delta t) = \tilde{g}_a^*(\mathbf{x}, t), \tag{22}$$

The LBM simulation is initialized by calculating Eq. (10–13) for the equilibrium distributions $\tilde{f}_a^{eq}$ and $\tilde{g}_a^{eq}$ at all lattice nodes in the domain using the initial velocity, density and temperature values. Then the effects of boundary conditions and forces (if any) are incorporated in order to calculate the unknown buffer distributions, $\tilde{f}_a^*$ and $\tilde{g}_a^*$, at the boundaries that are directed into the flow domain. First the boundary conditions at the open ends are imposed according to the pressure and temperature values specified at inlet and outlet. Then, no-slip and constant temperature boundary conditions are applied at

the walls. This is followed by the collision step where the direction-specific density distributions are relaxed toward quasi-equilibrium distributions. The equilibrium distributions are recomputed by Eq. (10–13), and The particles are streamed to the neighboring nodes by Eqs. (15,18). Finally the macroscopic flow properties are calculated at the next time step using Eq. (15–18). The pressure is related to density by $p = \rho c^2/3$ where the particle streaming speed is taken as $c = \sqrt{3RT_0}$ (assigned to 1 for now), where T_0 is the average temperature. The relation between the relaxation parameters is determined by the imposed Prandtl number, $Pr = \tau_p/\tau_g$.

2.1 Velocity and thermal boundary conditions

2.1.1 Inlet and Outlet Boundaries

Fig. 3 shows the various boundary conditions used in the current paper. For Couette flow (Fig. 3(a)) and for the force driven channel flow (Fig. 3(b)) periodic boundary conditions are applied at the inlet. For Poiseuille flow (Fig. 3(c)) and channel flow with a blockage (Fig. 3(a)) cases the a constant velocity and temperature profile is assigned at the inlet and at the exit the unknown distribution functions were extrapolated from the neighboring fluid nodes. To specify a constant temperature profile at the inlet boundary, the incoming unknown thermal populations ($\tilde{g}_1$, $\tilde{g}_5$, $\tilde{g}_8$) are assumed to be equilibrium distribution functions, with e_i thermal energy density imposed at the inlet. The unknown exit thermal populations facing the flow domain are set equal to those of the nearest interior nodes. To specify the velocity at the inlet, the idea of bounce-back of non-equilibrium part of the particle distribution function proposed by Zou and He [12]. The velocity component normal to the inlet

boundary is assumed to be zero and the density is to be determined. After streaming, at the inlet boundary ($\tilde{f}_1$, $\tilde{f}_5$, $\tilde{f}_8$) are unknown. Using Eqs. (), the density at the inlet ρ_i and unknown density functions are calculated as follows:

$$\rho_{in} = \frac{(\tilde{f}_9 + \tilde{f}_2 + \tilde{f}_4 + 2(\tilde{f}_3 + \tilde{f}_6 + \tilde{f}_7))}{(1 - u_i)}, \tag{23}$$

$$\tilde{f}_1 = \tilde{f}_3 + \frac{2}{3}\rho_{in}u_{in}, \tag{24}$$

$$\tilde{f}_5 = \tilde{f}_7 - \frac{1}{2}(\tilde{f}_2 - \tilde{f}_4) + \frac{1}{6}\rho_i u_i, \tag{25}$$

$$\tilde{f}_8 = \tilde{f}_6 + \frac{1}{2}(\tilde{f}_2 - \tilde{f}_4) + \frac{1}{6}\rho_i u_i, \tag{26}$$

In order to obtain the above equations, the bounce-back rule for the non-equilibrium part of the momentum density population normal to the inlet was used as, $\tilde{f}_1 - \tilde{f}_1^{eq} = \tilde{f}_3 - \tilde{f}_3^{eq}$.

2.1.2 Solid Boundaries

For the thermal conditions for the solid nodes, we follow a similar approach of Tang et al. [6] here. We demonstrate the procedure for the unknown energy distribution lower wall boundary depicted in Fig. 2. At the end of the collision step the unknown distributions at the lower wall boundary ($\tilde{g}_2, \tilde{g}_5, \tilde{g}_6$) must be calculated by Eq. (19, 20) however the unknown distribution functions at the solid nodes need to be calculated first. The distribution function $\tilde{g}_a(\mathbf{x}_{solid}, t)$ can be decomposed into its equilibrium and non-equilibrium parts by

$$\tilde{g}_a(\mathbf{x}_{solid}, t) = g_a^{eq}(\mathbf{x}_{solid}, t) + g_a^{neq}(\mathbf{x}_{solid}, t), \tag{27}$$

which is submitted into Eq. (20) in order to get

$$\tilde{g}_a^*(\mathbf{x}_{solid}, t) = (1 - \omega_g)g_a^{eq}(\mathbf{x}_{solid}, t) + \omega_g g_a^{neq}(\mathbf{x}_{solid}, t) - \omega_g \tau_g f_a h_a. \tag{28}$$

In order to calculate the non-equilibrium term $g_a^{neq}(\mathbf{x}_{solid}, t)$ it is assumed that $g_a^{neq}(\mathbf{x}_{solid}, t) = \epsilon g_a^1(\mathbf{x}_{fluid}, t)$ by using the Chapman-Enskog method, where ϵ is the expansion parameter. For the fluid nodes adjacent to the solid corner node in Fig. 2, $g_a(\mathbf{x}_{fluid}, t)$ can be determined by Eq. (9) since $\tilde{g}_a(\mathbf{x}_{fluid}, t)$ is known after the streaming step. The computed value of $g_a(\mathbf{x}_{fluid}, t)$ is used to find the non-equilibrium part of the distribution at the neighboring fluid node by $g_a^{neq}(\mathbf{x}_{fluid}, t) = \tilde{g}_a(\mathbf{x}_{fluid}, t) - g_a^{eq}(\mathbf{x}_{fluid}, t)$. This, in turn, is related to the non-equilibrium distribution at the solid node by $g_a^{neq}(\mathbf{x}_{solid}, t) = \tilde{g}_a^{neq}(\mathbf{x}_{fluid}, t) + O(\epsilon^2)$). The solid node equilibrium distribution in Eq. (20) is calculated by Eq. (10–13) using the $u = u_s$, $v = v_s$ and $e = e_s$ since no-slip and Dirichlet temperature boundary conditions are applied at the solid walls whereas the density value is obtained from the nearest fluid node. A similar procedure is followed for the no-slip velocity boundary condition at the solid nodes using $\tilde{f}_a(\mathbf{x}_{fluid}, t)$ instead of $\tilde{g}_a(\mathbf{x}_{fluid}, t)$.

3 Results

The accuracy of the TLBM is tested for thermal channel flows with various configurations as described in Fig. 3.

3.1 Thermal Couette flow

Couette flow with a temperature gradient provides a good test to describe viscous heat dissipation. With the bottom wall fixed and the top boundary moving at the speed of U_t, the temperature profile is given as

$$\frac{T - T_b}{T_t - T_b} = \frac{y}{H} + \frac{PrEc}{2}\frac{y}{H}\left(1 - \frac{y}{H}\right), \tag{29}$$

where T_b and T_t are the temperatures at the bottom and top boundaries, respectivle; y is the distance from the bottom boundary; H is the height of the channel; $Pr = \upsilon/\chi$ is the Prandtl number; and $Ec = U_t^2/c_v(T_1 - T_b)$ is the Eckert number. The effects of viscous heating are determined by Brinkmann number $Br = PrEc$ which represents the ratio between viscous dissipation and heat conduction. The flow is driven by the top wall moving at U_t while the top wall is kept at a higher temperature compared to the bottom wall ($T_t > T_b$). Periodic boundary conditions for both velocity and energy distributions were applied at the open boundaries. Fig. 4 shows the comparison of present results with the analytical solution for the temperature profile given by Eq. (29). In Fig. 4(a) the Prandtl number is fixed at $Pr = 2$ and the Eckert number is varied between $Ec = 10 - 100$ to obtain different Brinkmann number solutions. It was observed that as the Brinkmann number increases the non-linearity of the variation between the non-dimensional temperature profile is increased where the effect of viscous heating is felt mostly in the core region. Same effect is observed in Fig. 4(b) where the Eckert number is kept constant at $Ec = 100$ and Prandtl number is varied between $Pr = 0.5 - 5$. The present method was successful in predicting the temperature profiles compared with the analytical solution.

3.2 Thermal Poiseuille flow

A 2D planar flow driven by a constant body force F_x, with the walls at rest and at constant temperature $T_t = T_b$, is considered. At the open boundaries, periodic conditions are applied. The flow is initially at rest with a temperature

hotter than the wall temperature $T_f > T_t = T_b$. The analytical solution for temperature profile in the limit $Re = 0$ is given by [dorazio]

$$T(y) = T_b + \frac{(T_t - T_b)y}{H} + \frac{8PrU_M^2 y}{3c_v H}\left[\left(1 - \frac{3y}{H}\right) + 4\left(\frac{y}{H}\right)^2 - 2\left(\frac{y}{H}\right)^3\right] \quad (30)$$

where the center-line velocity U_M is related to the body force by

$$F_x = 8\rho_0 \nu U_M / H^2. \quad (31)$$

In Fig. 5(a) it is seen that the parabolic velocity profile is obtained. The TLBM solution for the normalized temperature profile is plotted in Fig. 5(b) where current TLBM results are found to be in good agreement with the analytical temperature profile given by Eq. 30. The corresponding normalized transverse heat flux profile is given in Fig. 5(c). In order to simulate a thermally developing channel flow, the same geometry is used with a constant velocity and temperature profile at the inlet boundary as depicted in Fig. 3(c). At the exit, the unknown distribution functions were extrapolated from the adjacent fluid nodes. The walls are kept at constant temperatures and the channel is cooled at the inlet, $T_i < T_t = T_b$. The local friction coefficient and local Nusselt number are plotted in Fig. 6. In the developed region of the channel the analytical values of $C_f Re = 24$ and $Nu = 7.54$ for hydraulically and thermally developed flows in straight channels are obtained by the TLBM.

3.3 Channel flow with a square blockage

The TLBM which was verified for flow and heat transfer in channel with straight walls in the previous section is further applied to simulate a channel including a square block in the flow domain (Fig. 3(d)). The boundary

conditions are same with the thermal Poiseuille flow case. In the current problem, the incoming fluid temperature is same with the wall temperature while the flow field is cooled by the square block which is kept at a lower temperature, $T_s < T_i = T_b = T_t$. For the unknown distribution functions at the surface of the square block, the same approach for wall boundaries given in Section 2.1.2 is used. The velocity contours for the steady-state flow field at an inlet Reynolds number of $Re_i = U_i(H-1)/\nu = 20$ is presented in Fig. 7(a). The channel dimensions are $H \times L = 91 \times 450$. Prandtl number selected is $Pr = 6$ with $\tau_f = 0.2$. The authors have shown in another study that the current settings simulate the characteristics of water with constant properties [11]. The ratio of the blockage height to channel width is $d/H = 0.356$. The flow speeds up through the gaps around the square block and then attain a parabolic profile at the downstream. The energy field contours are plotted in Fig. 7(b) for the same problem. The region of the channel downstream of the blockage is cooled by the square blockage. The upstream region of the blockage is not effected due to the dependence of convection on the velocity field. As the distance downstream of the blockage increases the temperature of the flow is increased due to the effect of the walls. The same problem is solved for a smaller blockage, $h/D = 0.1223$. The time evolution of the energy field is shown in Fig. 8. It is observed that the cooled region by the square block is reduced and the exit flow temperature is increased. In order to understand the effect of blockage size and the blockage temperature on the cooling effectiveness, the variation of the bulk temperature along the channel axial direction is plotted in Fig. 9. In Fig. 9(a) results for a channel with a blockage kept at a temperature of $T_s = 0.86T_i = 0.86T_w$ is presented. By reducing the size of the blockage from $d/H = 0.356$ to $d/H = 0.1223$ the exit temperature is increased by 0.59%. However, when the temperature of a blockage of $d/H = 0.356$ is re-

duced by half the exit boundary bulk temperature is reduced by 8% as shown in Fig. 9(b). This indicates that the temperature of the blockage has a more important role in cooling effectiveness compared to the size of the blockage.

4 Conclusions

In this paper the TLBM computations of incompressible flow and heat transfer in channels have been reported. The TLBM is first validated for the case of thermal Couette and thermal Poiseuille flow in a straight channel. Present computations were found to be in good agreement with the analytic solutions. Then the method has been successfully applied to analyze heat transfer in a channel with a square blockage. Comparative results suggest that the temperature of the cooling source in the channel plays a more important role compared to the size of the source. It is observed that the present method is a viable tool to model incompressible flows in channels including heat transfer.

References

[1] S. Chen, G. D. Doolen, Lattice Boltzmann Method for Fluid Flows, Annual Review of Fluid Mechanics 30 (1998) 329–364.

[2] Y. Peng, C. Shu, Y. T. Chew, Simplified thermal lattice Boltzmann model for incompressible thermal flows, Physical Review E 68 (2) (2003) 026701.

[3] A. D'Orazio, M. Corcione, G. P. Celata, Application to natural convection enclosed flows of a lattice boltzmann bgk model coupled with a general purpose thermal boundary condition, International Journal of Thermal Sciences 43 (6) (2004) 575 – 586.

[4] X. He, A Novel Thermal Model for the Lattice Boltzmann Method in Incompressible Limit, Journal of Computational Physics 146 (1998) 282–300.

[5] H. N. Dixit, V. Babu, Simulation of high Rayleigh number natural convection in a square cavity using the lattice Boltzmann method , International Journal of Heat and Mass Transfer 49 (2006) 727–739.

[6] G. H. Tang, W. Q. Tao, Y. L. He, Thermal boundary condition for the thermal lattice Boltzmann equation, Physical Review E 72 (1) (2005) 016703.

[7] A. D'Orazio, S. Succi, Simulating two-dimensional thermal channel flows by means of a lattice boltzmann method with new boundary conditions, Future Generation Computer Systems 20 (2004) 935 – 944.

[8] H. Huang, T. S. Lee, C. Shu, Thermal Curved Boundary Treatment for the Thermal Lattice Boltzmann Equation, International Journal of Modern Physics C 17 (2006) 631–643.

[9] Z. Guo, C. Zheng, B. Shi, An extrapolation method for boundary conditions in lattice boltzmann method, Physics of Fluids 14 (6) (2002) 2007–2010.

[10] C.-K. Chen, T.-S. Yen, Y.-T. Yang, Lattice boltzmann method simulation of backward-facing step flow with double plates aligned at angle to flow direction, Journal of Heat Transfer 128 (11) (2006) 1176–1184.

[11] S. Gokaltun, S. G. Dulikravich, Lattice boltzmann computations of incompressible laminar flow and heat transfer in a constricted channel, ASME-Journal of Heat Transfer(in works).

[12] Q. Zou, X. He, On pressure and velocity flow boundary conditions and bounceback for the lattice Boltzmann BGK model, Contributions to Mineralogy and Petrology (1996) 11001.

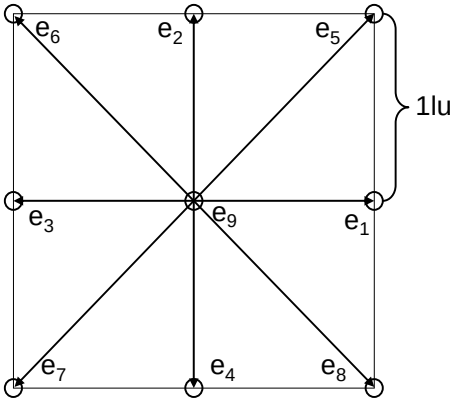

Fig. 1. The D2Q9 lattice structure.

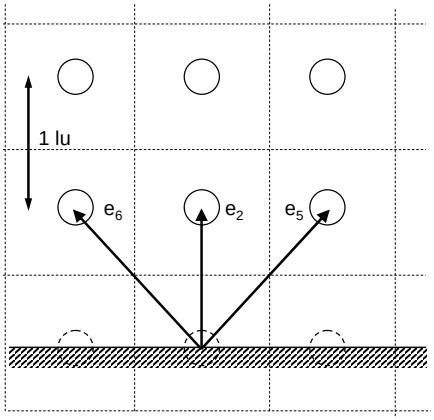

Fig. 2. Unknown density distribution directions at the wall boundary.

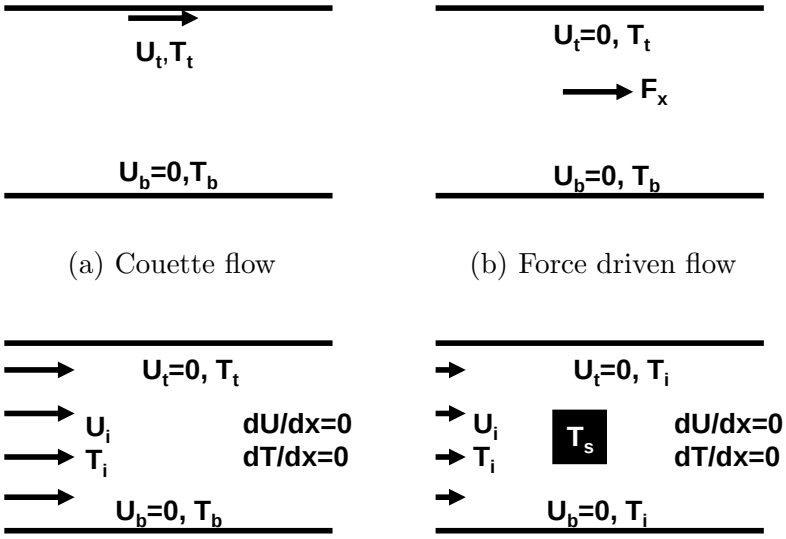

(a) Couette flow (b) Force driven flow

(c) Pouseuille flow (d) Channel with a square block

Fig. 3. Schematic showing the problems solved for straight channels.

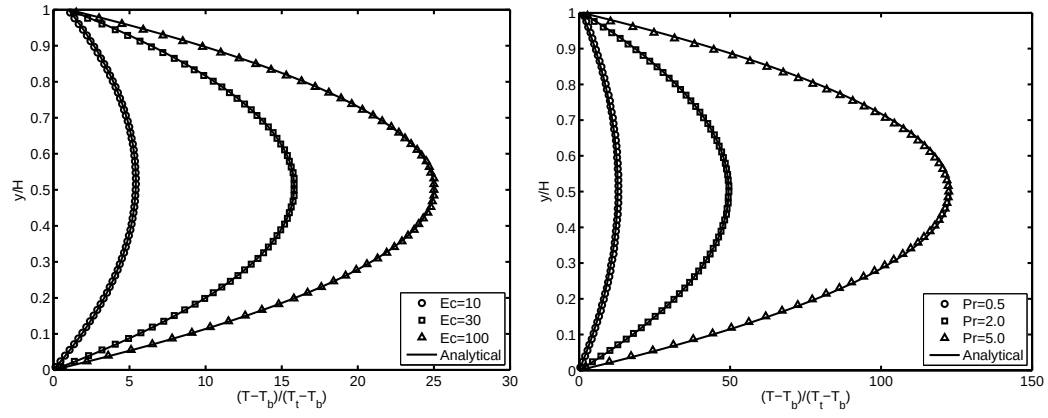

(a) $Pr = 2$ (b) $Ec = 100$

Fig. 4. Temperature profiles for various Pr and Ec numbers for thermal Couette flow.

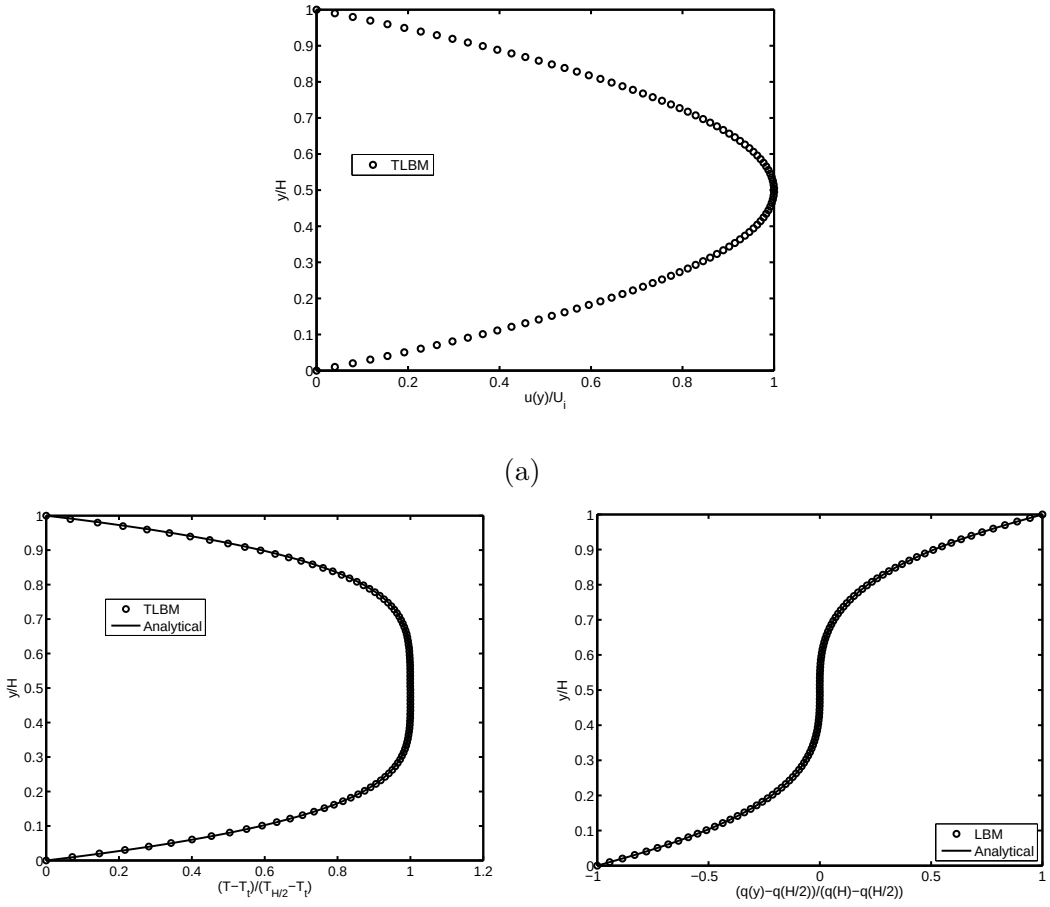

(a)

(b)

(c)

Fig. 5. Cross-sectional profiles in the force-driven channel flow for (a) velocity (b) temperature (c) heat flux.

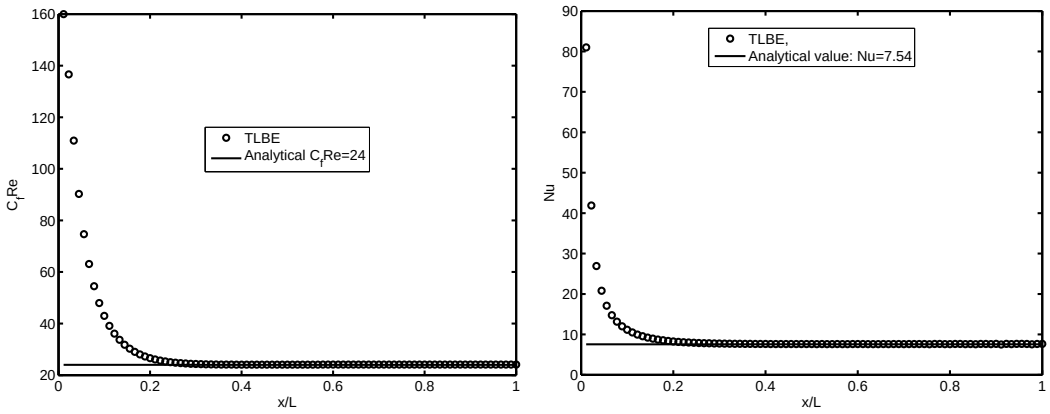

(a) (b)

Fig. 6. Local friction coefficient (a) and local Nusselt number (b) variation along the thermally developing channel.

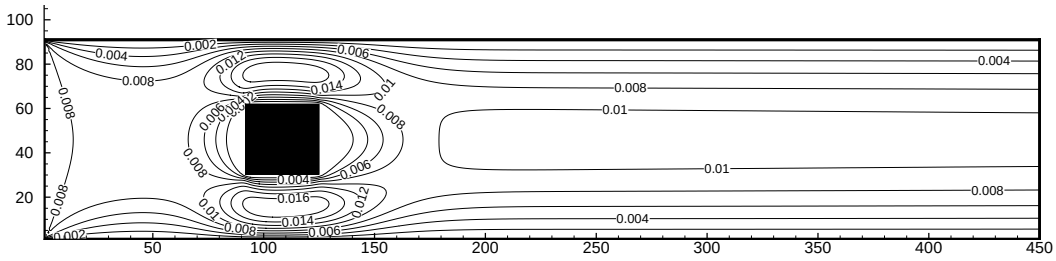

(a) Velocity field

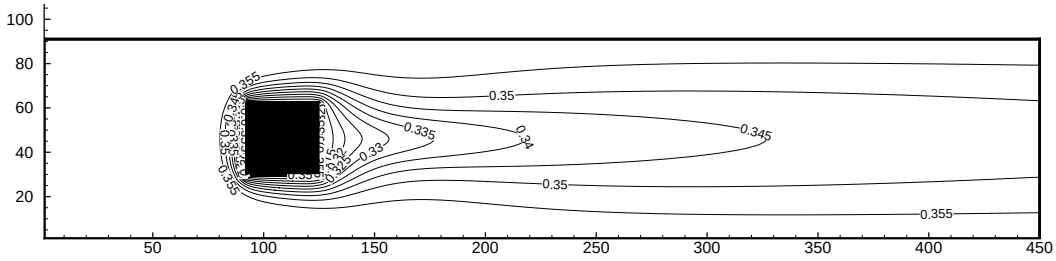

(b) Energy field

Fig. 7. Cooling of flow in a channel with a square block with a blockage size $d/H = 0.356$.

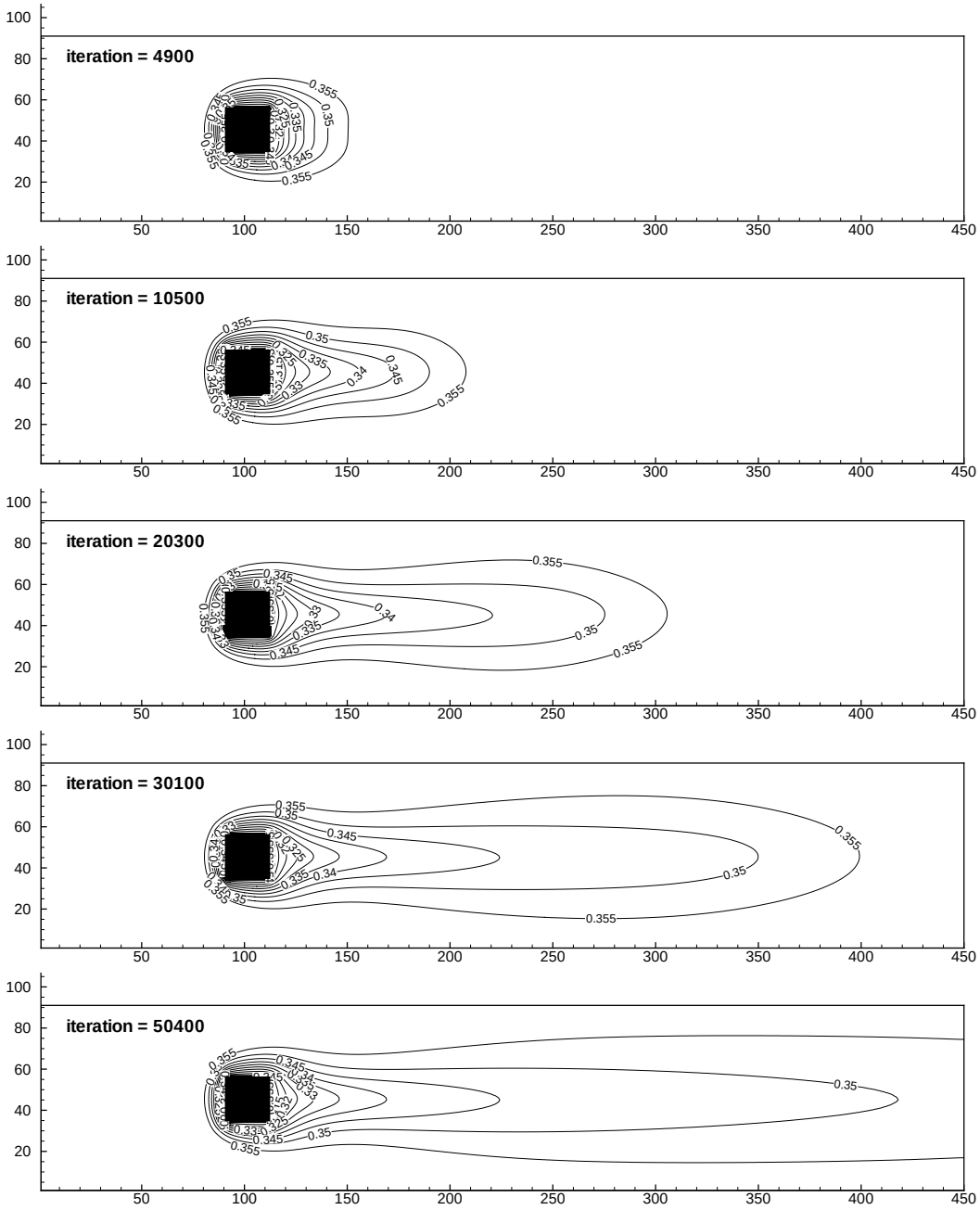

Fig. 8. Evolution of temperature field in a channel with a square block with $d/H = 0.1223$.

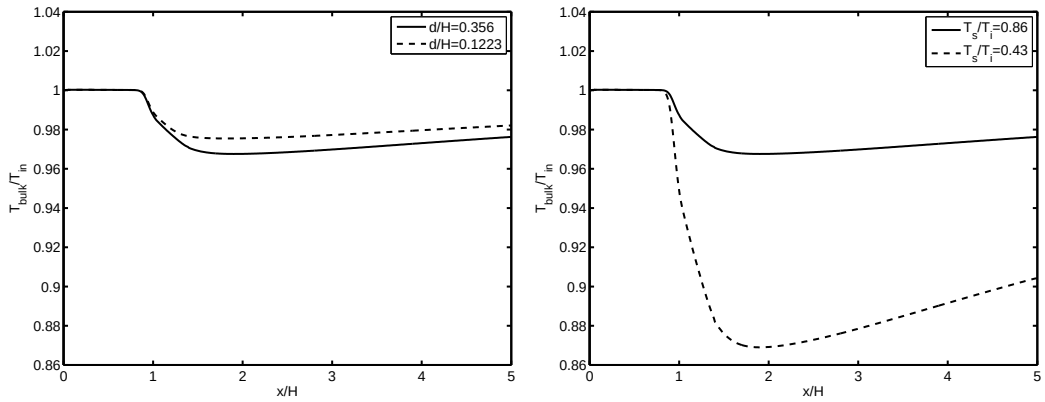

(a) $T_s/T_i = 0.86$ (b) $d/H = 0.356$

Fig. 9. Effects of blockage size and temperature on the energy field ($Re_i = 20$ and $Pr = 6$).